

~~How~~ Limitations in the use of atmospheric CO₂ ~~can inform us on~~ ~~annual and decadal shifts~~ observations to directly infer changes in the length of the biospheric carbon uptake period.

Theertha Kariyathan^{1,2}, Ana Bastos¹, Markus Reichstein¹, Wouter Peters^{2,3}, and Julia Marshall⁴

¹Max Planck Institute for Biogeochemistry, Germany

²Wageningen University and Research, Environmental Sciences Department, 6708 PB Wageningen, The Netherlands

³University of Groningen, Centre for Isotope Research, Groningen, The Netherlands

⁴Deutsches Zentrum für Luft- und Raumfahrt (DLR), Institut für Physik der Atmosphäre, Oberpfaffenhofen, Germany

Correspondence: Theertha Kariyathan (tkariya@bgc-jena.mpg.de)

Abstract. The carbon uptake period (CUP) refers to the time of each year during which the rate of photosynthetic uptake surpasses that of respiration in the terrestrial biosphere, resulting in a net absorption of CO₂ from the atmosphere to the land. Since climate drivers influence both photosynthesis and respiration, the CUP offers valuable insights into how the terrestrial biosphere responds to climate variations and affects the carbon budget. Several studies have assessed large-scale changes in CUP based on seasonal metrics from CO₂ mole fraction measurements. However, an in-depth understanding of the sensitivity of the CUP as derived from the CO₂ mole fraction data (CUP_{MR}) to actual changes in the CUP of the net ecosystem exchange (CUP_{NEE}) is missing. In this study, we specifically assess the impact of (i) atmospheric transport (ii) inter-annual variability in CUP_{NEE} (iii) regional contribution to the signals that integrate at different background sites where CO₂ dry air mole fraction measurements are made. We conducted idealized simulations where we imposed known changes (Δ) to the CUP_{NEE} in the Northern Hemisphere to test the effect of the aforementioned factors in CUP_{MR} metrics at ten Northern Hemisphere sites. Our analysis indicates a significant damping of changes in the simulated Δ CUP_{MR} due to the integration of signals with varying CUP_{NEE} timing across regions. CUP_{MR} at well-studied sites such as Mauna Loa, Barrow, and Alert showed only 50% of the applied Δ CUP_{NEE} under non interannually-varying atmospheric transport conditions. Further, our synthetic analyses conclude that interannual variability (IAV) in atmospheric transport accounts for a significant part of the changes in the observed signals. However, even after separating the contribution of transport IAV, the estimates of surface changes in CUP by previous studies are not likely to provide an accurate magnitude of the actual changes occurring over the surface. The observed signal experiences significant damping as the atmosphere averages out non-synchronous signals from various regions.

1 Introduction

Terrestrial ecosystems constitute a net sink of carbon from the atmosphere, mediated by the interplay between photosynthesis and respiration (autotrophic and heterotrophic). The period between the dates when an ecosystem transitions from being a carbon source to a carbon sink and vice-versa is referred to as the carbon uptake period (CUP) (Gonsamo et al., 2012). During the Northern Hemisphere's CUP, a continuous decline can be observed in atmospheric CO₂ mole fraction in many sites across

the globe. The CUP as defined by net ecosystem exchange (NEE) will be referred to as CUP_{NEE} and the corresponding period in the CO_2 mole fraction data will be referred to as CUP_{MR} . The timing and duration of the CUP_{NEE} and CUP_{MR} are influenced by vegetation phenology and soil respiration, which are in turn influenced by climate variability (Gill et al., 2015; Piao et al., 2019). For example in northern boreal and temperate ecosystems, warmer temperatures trigger early snowmelt and an associated early onset of plant growth in spring (Buermann et al., 2018; Zhou et al., 2020). In autumn, warm temperatures lead to delayed leaf senescence and a longer growing season (Piao et al., 2019; Shen et al., 2022). However, warmer temperatures can also enhance soil respiration if soil moisture is not limiting, and potentially result in earlier termination of the CUP_{NEE} and CUP_{MR} (Piao et al., 2008). The timing of the CUP_{MR} integrates the signal of ecosystem changes over large spatial scales. Metrics associated with CUP, e.g. its amplitude have been attributed to Northern Hemisphere greening (e.g. Forkel et al., 2016; Keeling et al., 1996; Barichivich et al., 2013) and to the intensification of the land carbon sink over the past decades (e.g. Graven et al., 2013; Ciais et al., 2019).

In previous studies (e.g. Fu et al., 2017, 2019), the CUP_{NEE} has been derived from eddy-covariance measurements of net CO_2 fluxes. However, estimation of the CUP_{NEE} using eddy-covariance flux measurements remains challenging on a global scale due to the uneven distribution of flux towers over the globe and the small spatial area covered by the footprint of these towers (Jung et al., 2020; Walther et al., 2022). Therefore, several studies have explored the potential of remote sensing to estimate the CUP_{NEE} (Churkina et al., 2005; Zhu et al., 2012; Gonsamo et al., 2012). However, while satellite-based indices provide information about the overall health and activity of vegetation, they cannot distinguish between different components of the carbon cycle, such as gross primary production (GPP) and ecosystem respiration. In drought-stressed ecosystems, there may even be periods of carbon release during the growing season (Churkina et al., 2005; Zhu et al., 2012; van der Woude et al., 2023), influencing CUP_{NEE} . The satellite-based indices are closely related to vegetation growth or photosynthesis and characterize the start and end of the growing season (Wang et al., 2022; Zeng et al., 2020), but they do not necessarily capture CUP_{NEE} .

Measurements of atmospheric CO_2 dry air mole fraction from remote background sites represent the balance between surface emissions and uptake from land and ocean (Keeling et al., 1996) over large spatial scales. The seasonal patterns evident in these data from the Northern Hemisphere, reflect the terrestrial ecosystem exchange mostly from the high and mid-latitudes and have been used by previous studies to investigate the changes in the CUP_{NEE} over large spatial scales (e.g. Barichivich et al., 2012; Piao et al., 2008, 2017). Robust methods were developed for estimation of the CUP from CO_2 mixing ratio, such as the Ensemble of First Derivative (EFD) method from Kariyathan et al. (2023), that was better able to identify changes in the CUP_{NEE} compared to the conventional use of the dates when the detrended seasonal cycle crossed the zero-value. Even with refined CUP_{MR} estimation methods, atmospheric transport causes a significant fraction of observed CO_2 variations at surface stations. Inter-annual variations and long-term trends in atmospheric transport can affect the relationship between the seasonal cycle of atmospheric CO_2 observations and surface exchange (Murayama et al., 2007; Piao et al., 2008). ~~Previous studies~~ by For example, Jin et al. (2022) studied the impact of varying winds and ecological CO_2 fluxes on seasonal cycle amplitude trends, finding that shifting winds partially offset the amplitude increase at MLO, contributing nearly 50% to the seasonal

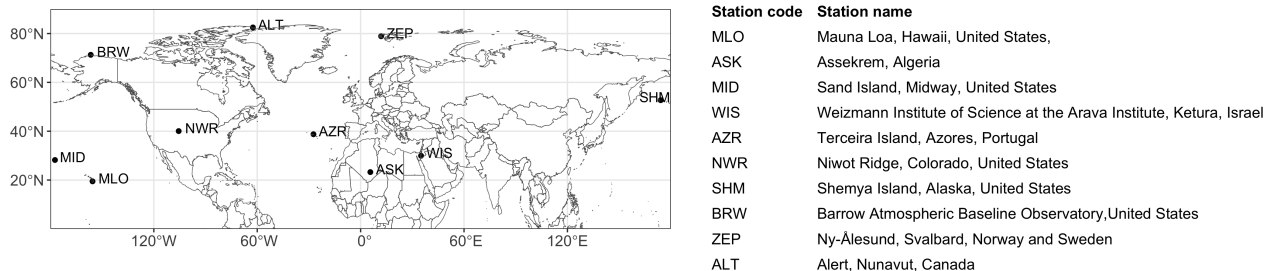


Figure 1. Map showing the location of studied sites, with the station names corresponding to the station code shown in the map.

[cycle amplitude changes between 1959 and 2019](#). Lintner et al. (2006) suggest a contribution by atmospheric transport to the downward trend in the CO₂ seasonal cycle amplitude observed at Mauna Loa (MLO) between 1991 and 2002. Murayama et al. (2007) demonstrated how year-to-year changes in atmospheric transport create significant inter-annual variations in the downward zero-crossing date of the CO₂ seasonal cycle, inevitably influencing CUP_{MR} estimates. [Here Previous studies have primarily focused on aspects such as the seasonal cycle amplitude or zero-crossing times. Barlow et al. \(2015\) have used the improved CUP estimation method and explored the influence of transport on CUP timing to some extent. In this study, we aim to understand in detail how well the CUP_{MR} deduced from atmospheric time series observations of CO₂ mixing ratios represents the CUP_{MR} changes from the Northern Hemisphere biosphere and its inter-annual variability \(IAV\), especially:](#)

- 1 To what extent do CO₂ mixing ratio observations accurately capture variations in CUP_{NEE}?
- 2 How does IAV in atmospheric transport affect the observed changes in CUP_{MR}?
- 3 Considering the variability in both CUP_{NEE} and transport, can CUP_{MR} effectively reflect long-term trends in CUP_{NEE}?
- 4 Can the changes observed at the studied sites be attributed to specific regions of the Northern Hemisphere?

To address these questions, we evaluate the role of transport in shaping the CUP_{MR} at regional and global scales, by conducting a series of experiments using the atmospheric transport model TM3 (Heimann and Körner, 2003) for a total of ten sites in the Northern Hemisphere (Fig. 1).

2 Methods

To evaluate the degree to which CUP_{MR} represent the changes in the CUP_{NEE}, when influenced by atmospheric transport, we design idealized scenarios with prescribed changes to the optimized net ecosystem exchange (NEE) fluxes from the Jena Carboscope Atmospheric CO₂ Inversion (Rödenbeck et al., 2003) (version ID: sEXT_ocNEET_v2021). The modifications were applied solely to pixels in the Northern Hemisphere (> 0° N) with a clearly defined seasonal cycle, characterized by a

Table 1. Description of different forward simulation experiments, using manipulated NEE fluxes. The first character in the experiment name indicates if the early (E) or late (L) CUP_{NEE} phases are manipulated, the next character specifies if Northern Hemisphere (N) or Regional (R) fluxes are adjusted and the subscript and superscript of the last character denote variability (V) in ~~transport and~~ CUP_{NEE} ~~and transport~~ respectively. The Δ applied in each experiment is shown in the first column. In Δ_x^d CUP_{NEE}, x ranges from -10 to +10 days in intervals of two days. In Δ_x^l CUP_{NEE}, x can be a sequence from -10 to +10 days and vice versa denoted by p and n respectively in the main text.

Δ CUP _{NEE}	Period	Spatial Structure	CUP _{NEE}	Transport	Experiment
Discrete (Δ_x^d)	Early (E)	Northern Hemisphere (NH)	Fixed (V_0)	Fixed (V^0)	ENV_0^0
		Regional (R)	Fixed	IAV (V^T)	ENV_0^T
				Fixed	ERV_0^0
	Late (L)	Northern Hemisphere	Fixed	IAV	ERV_0^T
				Fixed	LVN_0^0
		Regional	Fixed	IAV	LVN_0^T
Linear (Δ_x^l)	Early	Northern Hemisphere	Fixed	Fixed	LRV_0^0
		Regional	Fixed	IAV	LRV_0^T
	Late	Northern Hemisphere	Fixed	IAV	ENV_0^T
		Regional	Fixed	IAV	LVN_0^T
	Early	Northern Hemisphere	Fixed	IAV	ENV_0^T
		Regional	Fixed	IAV	ENV_1^T
		Northern Hemisphere	IAV (V_1)	IAV	ERV_1^T
		Regional	IAV	IAV	ERV_1^T
	Late	Northern Hemisphere	IAV	IAV	LVN_1^T
		Regional	IAV	IAV	LRV_1^T
	Early	Northern Hemisphere	2 times IAV (V_2)	IAV	ENV_2^T
		Regional	2 times IAV	IAV	LVN_2^T

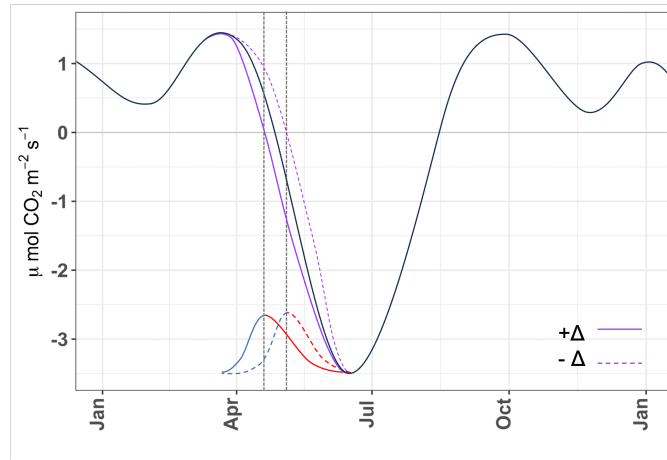


Figure 2. Schematic showing manipulation of CUP_{NEE} . The shifted purple solid/dashed curves result in $+\Delta$ and $-\Delta$ changes in the CUP_{NEE} , respectively. The curve is obtained by subtracting/adding two half-Gaussian curves. For example, the red and blue curves combine at the points (i.e., new onset) indicated by the dashed black lines to produce the purple curves (described in Sect. 2.3). The seasonal cycle minimum separates the early (left) and late (right) CUP_{NEE} phases. The manipulation for the early CUP_{NEE} phase is shown here and can be similarly applied to the late CUP_{NEE} phase.

seasonal cycle minimum, and downward and upward zero-crossing points in spring and autumn, respectively. The year 2003 is employed as the reference year (simulations with an alternative reference year, 2001, did not show a noticeable difference), and pixels exhibiting clearly defined seasonal cycles in that specific year were chosen for perturbation. For the remaining pixels, the reference year flux was repeated over time, so that there was no IAV in CUP_{NEE} . This was done to ensure that any observed changes in the simulated CO_2 mixing ratio could be attributed to the prescribed Δ . The influence of fossil fuel, biomass burning, and ocean fluxes on the seasonal variation of atmospheric CO_2 is minimal, and changes in the seasonal cycle of atmospheric CO_2 reflect alterations in the integrated net ecosystem exchange in the Northern Hemisphere (Barichivich et al., 2012).

While these fluxes were not modified in our simulations, our results are based on differences between simulations where only the NEE flux is altered. The flux manipulation was carried out from 1995 to 2017, aligning with the meteorological forcing used in the transport model. These adjusted fluxes were then transported forward using an atmospheric transport model, TM3 (Heimann and Körner, 2003), simulating time series of CO_2 mixing ratios at different study sites (as shown in Fig. 1), in temporal frequency aligning with the flask measurements at the sites. After the forward transport run, we assess CUP_{MR} changes based on the simulated CO_2 mixing ratios (ΔCUP_{MR}) resulting from ΔCUP_{NEE} . We use the ensemble of the first derivative (EFD) method from Kariyathan et al. (2023) to evaluate CUP_{MR} , as its efficacy on the sites shown in Fig.1 was previously established in Kariyathan et al. (2023). The method uses an ensemble-based approach to quantify the uncertainty associated with curve-fitting discrete time series data and deriving seasonal cycle metrics. Using this approach, an optimal threshold is defined based on the first derivative of the CO_2 seasonal cycle to determine CUP timing. The threshold is selected such that the CUP timing closely corresponds to the spring maximum and late summer minimum, with minimal influence from curve-fitting

uncertainty caused by multiple or broader peaks in the CO₂ seasonal cycle.

To evaluate how well CUP_{MR} captures the changes in CUP_{NEE}, we used ~~experiment~~ experiments ENV_0^0 and LV_0^0 , where we imposed spatially uniform, discrete changes in CUP_{NEE} (Δ^d) and the atmospheric transport was held constant in the forward transport run (meaning that one year (2008) of transport was repeated). Then to answer how the IAV in atmospheric transport affects derived CUP_{MR}, the CO₂ mixing ratios were simulated with inter-annually-varying meteorology (experiment ENV_0^T and LV_0^T). To evaluate the ability of CUP_{MR} to reflect long-term trends in CUP_{NEE}, we initially assessed the ability to capture a trend in CUP_{NEE} while accounting for IAV in atmospheric mixing. This was achieved by prescribing long-term trends in CUP_{NEE} (Δ^l) and conducting the forward transport run with inter-annually varying meteorology. Subsequently, we then test the detectability of prescribed linear trends in CUP_{NEE} (Δ^l) when IAV was present in both atmospheric transport and NEE (experiments ENV_1^T and LV_1^T). Additionally, to analyze the influence of IAV in CUP_{NEE}, we prescribed known IAV to CUP_{NEE} (experiments ENV_2^T and LV_2^T). Further, to understand the sensitivity of the simulated signals to regional changes (experiments ERV_0^0 , LRV_0^0 , ERV_1^T and LRV_1^T), we limited the flux ~~manipulation to the different aggregated~~ 5 Northern Hemisphere land regions of the TransCom3 (Gurney et al., 2002) experiment, namely Europe, Eurasian Temperate, Eurasian Boreal, North American Temperate and North American Boreal. The experiments performed are listed in Table 1.

2.1 NEE flux manipulation

The CUP_{NEE} is the period when the NEE flux is negative, and the downward and upward zero-crossing dates represent the onset and termination of the CUP_{NEE} respectively. Hence, we shift the NEE zero-crossing dates to have a change Δ (where Δ is measured in days) in the CUP_{NEE} duration (Δ CUP_{NEE}). The NEE flux is characterized by daily temporal resolution, showing relatively gradual variations along the y-axis compared to the x-axis. For all the experiments performed, the NEE values (i.e., y-axis) are modified to achieve the desired timing adjustments (Δ) in CUP_{NEE}, without altering the time axis itself. This adjustment ensures the creation of a smooth curve that closely mirrors the actual flux while achieving the intended change in CUP_{NEE}. For each value of Δ CUP_{NEE}, we modify the downward and upward zero-crossing dates of NEE separately, to evaluate the effect of changes in the early and late CUP_{NEE} phases respectively. This is achieved by adding or subtracting a continuous curve to the period extending from the peak in spring to the NEE minimum for early phase changes and the period from the NEE minimum to peak in winter for late phase changes. The curve is created by combining two distinct half Gaussian curves (Fig. 2, red and blue curves): the first curve has its peak at the new onset/termination and a standard deviation (σ_1) equal to one-third of the distance between the NEE peak in spring/winter and the new onset/termination. The second curve, also with its peak at the new onset/termination, has a different standard deviation (σ_2) equal to one-third of the distance between the new onset/termination and the date corresponding to the NEE minimum value. This configuration (i.e., Gaussian peaks and σ) ensures that the Gaussian tail minimizes any shift around the NEE peak and trough while realizing the Δ shift at the onset or termination of the CUP_{NEE}.

Some pixels exhibit a distinct seasonal pattern without a well-defined peak in spring or winter. In those cases, the period

130 for manipulating the early and late CUP phases then extends from the beginning of the year to the day of minimum NEE and from the day of minimum NEE to the end of the year, respectively. The portions of the first and second curves corresponding to the range from " $\mu - 3\sigma_1$ " to " μ " and from " μ " to " $\mu + 3\sigma_2$," respectively, are then combined and smoothed using a spline function (Fig. 2, purple curves).

135 We note that the annual flux is not conserved in the manipulation. However, we detrend the simulated CO₂ mixing ratio prior to CUP_{MR} analysis, which would remove any trend in the CO₂ mixing ratio caused by repetition of the manipulated years. Further, when evaluating the simulated CO₂ time series, we found that the change in the total annual flux only changes the peak-to-peak amplitude and does not influence the timing and duration of the simulated time series, except at times corresponding to periods of manipulation in the CUP_{NEE}. This happens for instance, when the downward zero crossing of the
140 NEE flux is manipulated, it changes only the CUP onset and has minimal influence on the CUP termination in the CO₂ mixing ratios. The different cases of manipulation are described below:

1. Δ_x^d : In these simulations, every year has the same discrete change in CUP_{NEE}. In the different experiments, the magnitude of the shift (denoted by x) ranges from -10 to 10 days in intervals of 2 days.
2. Δ_x^l : In these simulations, Δ CUP_{NEE} progresses from -10 days to +10 days (denoted by $x = p$) or vice versa (denoted by
145 $x = n$) over the period of manipulation.

Manipulation Δ_x^d is done for experiments where there is no IAV in CUP_{NEE}, indicated by V_0 in the experiment name. Δ_x^l manipulation is made for experiments with and without IAV in CUP_{NEE} (i.e., experiment names with V_0 , V_1 and V_2). For the case V_0 , the manipulation is done on the flux of a reference year (chosen arbitrarily 2003), which is repeated in time so that there is no IAV in CUP_{NEE}. Any IAV in CUP_{MR} may then be attributed to IAV in transport. In V_1 , the annual fluxes are used
150 instead of repeating the base year flux. The case V_2 has a prescribed IAV in CUP_{NEE}. For a given pixel, a set of Δ values is added to the original CUP_{NEE} in the manipulation period (2000-2017). The set of Δ has a mean zero and a standard deviation twice that of the IAV in the original CUP_{NEE} for the manipulation period.

The flux alteration is complicated to apply in some cases, as described below :

- 155 1. When a local maximum is observed between the downward or upward zero-crossing points and the minimum NEE. In such cases, adding the Gaussian curve shifts these peaks above the zero-crossing line, creating an additional downward or upward zero-crossing point. This complicates the assessment of CUP_{NEE} following the manipulation, and results in Δ CUP_{NEE} being different from the prescribed value. The Δ is kept at zero in this case.
2. In a few instances, when the magnitude of Δ is larger than the period between the original zero-crossing dates and the
160 start/end of the period of manipulation, we instead opt for the next-closest Δ value in the sequence.
3. Additionally, in manipulation cases where inter-annually varying fluxes are used (Δ_x^l), only certain years have the complexities described above. In such instances, the next available Δ value from the sequence is chosen to minimally

impact the imposed CUP_{NEE} trend. This involves selecting a Δ such that it results in a smaller or larger value compared to the subsequent year, achieving either a positive or negative change in CUP_{NEE} (i.e., Δ_p^l or $\Delta_n^l CUP_{NEE}$).

165 [The manipulated pixels for the different cases are shown in Fig. 3.](#) Furthermore, the manipulated fluxes are used to conduct regional sensitivity analyses, in which we limit the flux manipulation process explained above to different TransCom3 (Gurney et al., 2002) geographic regions in the Northern Hemisphere. This allows us to evaluate the regional contribution of NEE fluxes to ΔCUP_{MR} when comparing how perturbations involving different regions are expressed in $\Delta_x^l CUP_{MR}$ at the studied sites. This comparison is conducted for two experiments: ERV_0^0 , illustrating the integration of signals from various regions
170 in an idealized scenario without IAV in atmospheric transport or CUP_{NEE} ; and ERV_1^T , which reflects signal integration in a relatively realistic setting, with IAV in atmospheric transport and CUP_{NEE} .

2.2 Forward transport runs

We use a three-dimensional global atmospheric transport model, TM3 (Heimann and Körner, 2003), to simulate CO_2 mixing ratios at the specified sites based on manipulated NEE fluxes. The model is run at a spatial resolution of 5° in longitude and
175 4° in latitude with 19 vertical levels, using 6-hourly NCEP reanalysis meteorological fields from 1995 to 2017 and daily surface fluxes from the Jena Carboscope CO_2 Inversion (version ID: sEXT_ocNEET_v2021) (Rödenbeck et al., 2003), with the NEE fluxes manipulated as previously described. The forward runs are carried out with 1) fixed transport (meteorology from a random year, here we used the year 2008 and repeated it in time such that there is no IAV) and 2) with inter-annually varying transport for the period 1995 to 2017 to study the contribution of atmospheric transport to the IAV in CUP_{MR} . The first five
180 years are excluded from the CUP_{MR} analysis to account for the model's spin-up time, and ΔCUP_{NEE} is held at zero during this period.

2.3 CUP estimation methods

The forward transport runs simulate CO_2 mixing ratios at discrete time steps, which we sample at the frequency corresponding to the flask measurements (approximately bi-weekly) at the studied sites. [This sampling interval sufficiently captures the
185 larger-scale trends and seasonal variations critical to our analysis and allows for consistent comparison with previous studies that looked into long-term trends using flask measurements.](#) We apply the ensemble of first derivative (EFD) method described in Kariyathan et al. (2023) to the output data and estimate the CUP_{MR} . Here, the CUP_{MR} is estimated using a threshold, derived from the first derivative of the detrended and smoothed CO_2 mixing ratio seasonal cycle curves. A threshold of 15% and 0% of the first-derivative minimum was used as a threshold to determine the onset and termination of the CUP_{MR} , respectively, as in
190 Kariyathan et al. (2023). The calculation is applied to an ensemble of the detrended time series, which allows for an uncertainty range on the CUP estimate to be calculated.

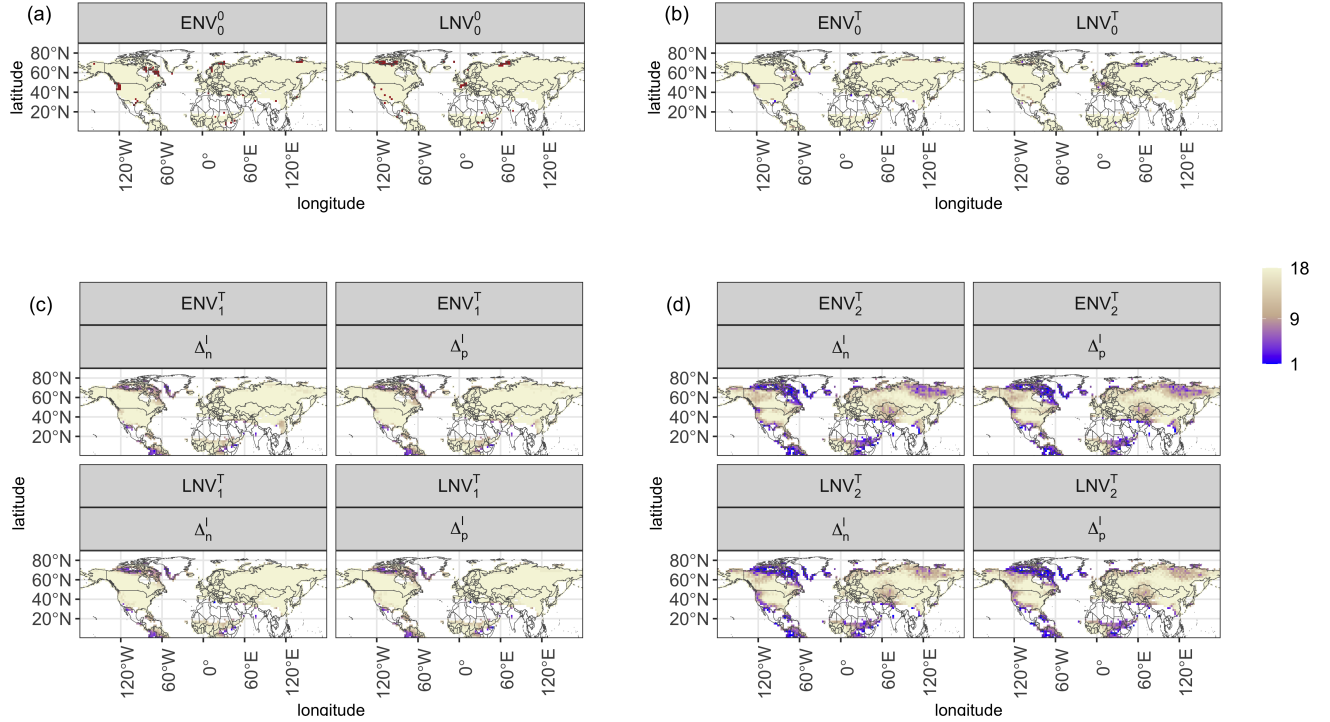


Figure 3. Spatial distribution of the pixels manipulated for different experiments: (a) reference year flux is repeated and discrete changes are prescribed to CUP_{NEE} (beige), the red color represents pixels where Δ is different from the prescribed Δ due to the complications described in Sect. 2.1. (b) reference year flux is repeated and a long-term trend is applied to CUP_{NEE} . When a long-term trend is applied, Δ varies over the years. The color bar indicates the number of years for which Δ equals the prescribed Δ i.e., years with no complications described in Sect. 2.1 (also applicable for panels (c) and (d)). (c) actual CUP_{NEE} is retained and long-term trend is applied to CUP_{NEE} . (d) IAV in CUP_{NEE} is doubled and a long-term trend is applied. The panel titles in every plot represent different simulations as detailed in Table 1.

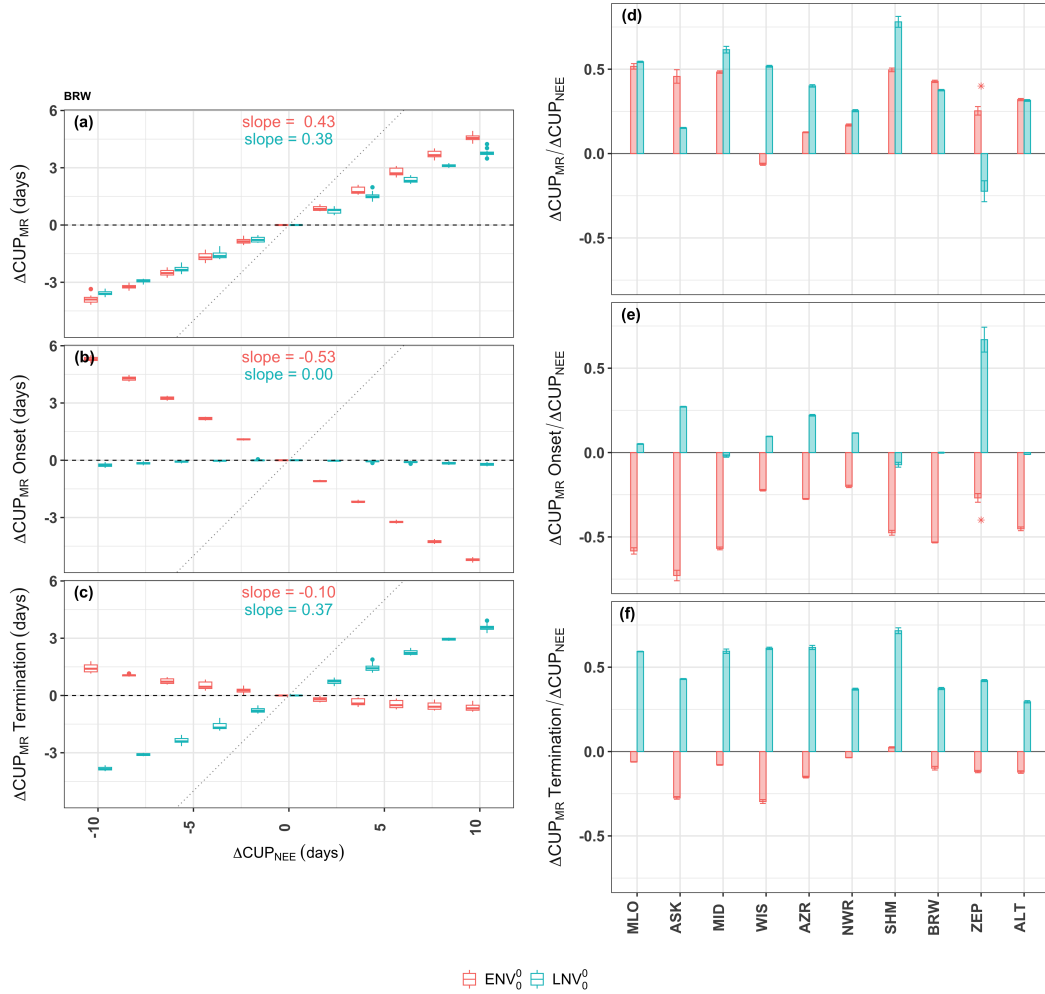


Figure 4. The change in CUP_{MR} metrics in response to varying ΔCUP_{NEE} for experiments ENV_0^0 (red) and LVN_0^0 (cyan). The experiments ENV_0^0 and LVN_0^0 largely drives the Δ in CUP_{MR} onset and termination respectively and thereby ΔCUP_{MR} . The left panel shows panels show, the Δ in (a) CUP_{MR} (ie., the duration), (b) CUP_{MR} onset and (c) CUP_{MR} termination against the applied ΔCUP_{NEE} for BRW. In these panels, the individual boxplot displays boxplots display the distribution of the median metrics values across years, estimated from the ensemble spread for each year. The distribution dotted line represents an ideal case of the boxplots against a one-to-one relation between ΔCUP_{NEE} shows deviation from the one-to-one relation (shown by the dotted line) and ΔCUP_{MR} . The text within these plots shows the slope of the regression lines fitted to the median of the boxplots. The right panel panels ((d) to (f)) shows show these slopes (unit less) across the different studied sites. The estimate of ZEP is reduced to 0.1 times the actual value for ease of visualization. Error bars represent \pm one standard deviation (σ) around the estimated slope.

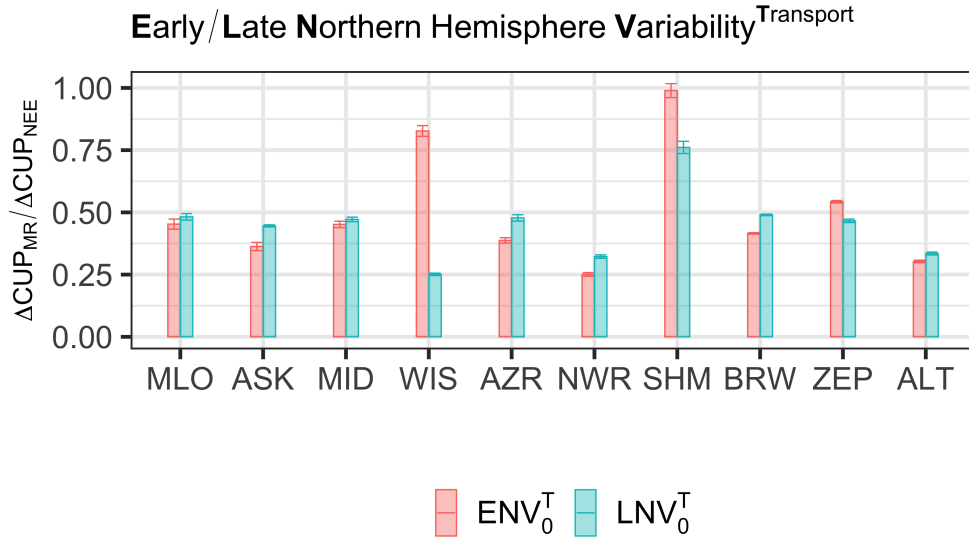


Figure 5. The change in CUP_{MR} metrics in response to varying $\Delta\text{CUP}_{\text{NEE}}$, similar to Fig. 4, (d) but for the experiments with inter-annually varying meteorology, ENV_0^T (red) and LNV_0^T (cyan).

3 Results

3.1 Northern Hemisphere CUP_{MR} sensitivity under fixed transport

The calculated $\Delta\text{CUP}_{\text{MR}}$ consistently shows lower absolute values than the prescribed $\Delta\text{CUP}_{\text{NEE}}$. For example, at BRW, $\Delta\text{CUP}_{\text{MR}}$ is 0.43 times the prescribed early phase $\Delta\text{CUP}_{\text{NEE}}$ as illustrated in Fig. 4, (a). This reduction in $\Delta\text{CUP}_{\text{MR}}$ is found across all the studied sites with varying degrees of intensity as illustrated in Fig. 4, (d), when Δ is prescribed to either the early or late phases of CUP_{NEE}. This shows how atmospheric observations respond differently to CUP perturbations compared to local NEE measurements, and a one-on-one translation might lead to an incorrect interpretation of at least the magnitude of CUP changes. The persistent difference in the magnitude of $\Delta\text{CUP}_{\text{MR}}$ from the imposed $\Delta\text{CUP}_{\text{NEE}}$ results from the integration of signals from various regions with different CUP_{NEE} timings as detailed in Sect. 4.

At most studied sites, the Δ assigned to the early phase of CUP_{NEE} predominantly affects the onset of CUP_{MR} (Fig 4, (b) and (e)). The $\Delta\text{CUP}_{\text{MR}}$ then corresponds to the changes in onset of CUP_{MR} as indicated by the similar variation in the red bars in Fig. 4 (d) and (e). Similarly, Δ applied to the late phase of CUP_{NEE} primarily influences the termination of CUP_{MR} (Fig. 4, (c) and (f)) which then drives $\Delta\text{CUP}_{\text{MR}}$ in experiment LNV_0^0 (Fig. 4, (d) and (f), cyan bars). This suggests that the changes in the early and late phases of CUP at the surface can be analyzed separately by examining the onset and termination of CUP inferred from CO₂ mole fraction observations. Contrary to the direct but dampened relationship between $\Delta\text{CUP}_{\text{NEE}}$ and $\Delta\text{CUP}_{\text{MR}}$, we find an opposite response at some sites: a lengthening (shortening) imposed on CUP_{NEE} leads to shortening

(lengthening) of the CUP_{MR} . This is seen to occur at sites ZEP and WIS, as indicated by the negative slopes at these sites (Fig. 4, (d)).

At ZEP, the late phase ΔCUP_{NEE} leads to unintended changes in CUP_{MR} onset. For Δ prescribed to the late CUP_{NEE} phase, the change in CUP_{MR} termination is only 0.4 times the Δ , while that in the onset is 0.6 times the Δ . Thus, the changes intended for CUP_{MR} termination extend to CUP_{MR} onset in the following year. For example, a 10-day delay prescribed to the CUP_{NEE} termination results in a 4-day delay in CUP_{MR} termination and a 6-day delay in the onset. This results in a 2-day shorter CUP_{MR} , establishing an inverse relation between ΔCUP_{MR} and ΔCUP_{NEE} at ZEP (slope of -0.22 in the experiment $LN V_0^0$). Likewise, at WIS, in experiment $EN V_0^0$, the change in CUP_{MR} onset is only -0.2 times the applied early phase ΔCUP_{NEE} , while the change in termination is -0.3 times the perturbation imposed. This offsets the ΔCUP_{MR} and leads to a significant ($p < 0.001$) inverse relation between ΔCUP_{MR} and ΔCUP_{NEE} at WIS (slope of -0.06, in the $EN V_0^0$ experiment).

220 3.2 Northern Hemisphere CUP_{MR} sensitivity under inter-annually varying transport

Even when interannual variations from atmospheric transport are included, changes imposed in ΔCUP_{NEE} are reflected in ΔCUP_{MR} . The varying atmospheric transport leads to year-to-year variations in signal integration and changes that were not captured in the experiment with transport from single-year meteorology can be seen in the experiment with inter-annually varying transport. This is illustrated for different sites in Fig. 5. An inverse relation between ΔCUP_{MR} and ΔCUP_{NEE} was calculated at WIS and ZEP in experiments $EN V_0^0$ and $LN V_0^0$, respectively, as described in Sect. 3.1. However, in experiments with varying transport, slope values of 0.83 at WIS (experiments $EN V_0^T$) and 0.47 at ZEP (experiment $LN V_0^T$) are found, compared to -0.06 and -0.22 in the experiment with fixed transport. This suggests that anomalies observed in specific years may be predominantly attributed to the meteorological conditions of those particular years.

3.3 Northern Hemisphere CUP_{MR} sensitivity to long-term trends in CUP_{NEE}

230 Out of all the evaluated sites, only SHM and BRW partially captured CUP_{MR} trends corresponding to the imposed trends in CUP_{NEE} (Fig. 6 as shown in Fig. 6 (results for other sites are shown in Table A1)). In experiment $EN V_0^T$, the largest trend in CUP_{MR} is derived at SHM, with values of 0.5 days/year and -0.3 days/year for the imposed increasing (1.11 days/year) and decreasing (-1.11 days/year) trend respectively. Similarly, in experiment $LN V_0^T$, the largest trend in CUP_{MR} is observed at BRW (0.5 days/year and -0.2 days/year for the imposed increasing and decreasing trend respectively). Nevertheless, part of the observed trend can be attributed to the IAV in atmospheric transport thereby showing that the IAV in transport can influence our understanding of the actual long-term changes in CUP_{NEE} trends. This can be seen in Fig. 6, green bars (Δ_0^I), corresponding to experiments $EN V_0^T$ and $LN V_0^T$. Note that in these experiments, there is no IAV in the CUP_{NEE} flux as indicated by the subscript '0', and Δ_0^I indicates that no trend is prescribed to the CUP_{NEE} . Then any derived CUP_{MR} trend can be attributed solely to the IAV in transport. The trend from the IAV in transport then leads contributes to the asymmetry between the red and blue bars. At BRW, experiment $LN V_0^T$, indicates that a CUP_{MR} trend of 0.1 days/year can arise from variability in transport alone, and accounts for about 20% of the derived CUP_{MR} trend (blue bar showing 0.5 days/year).

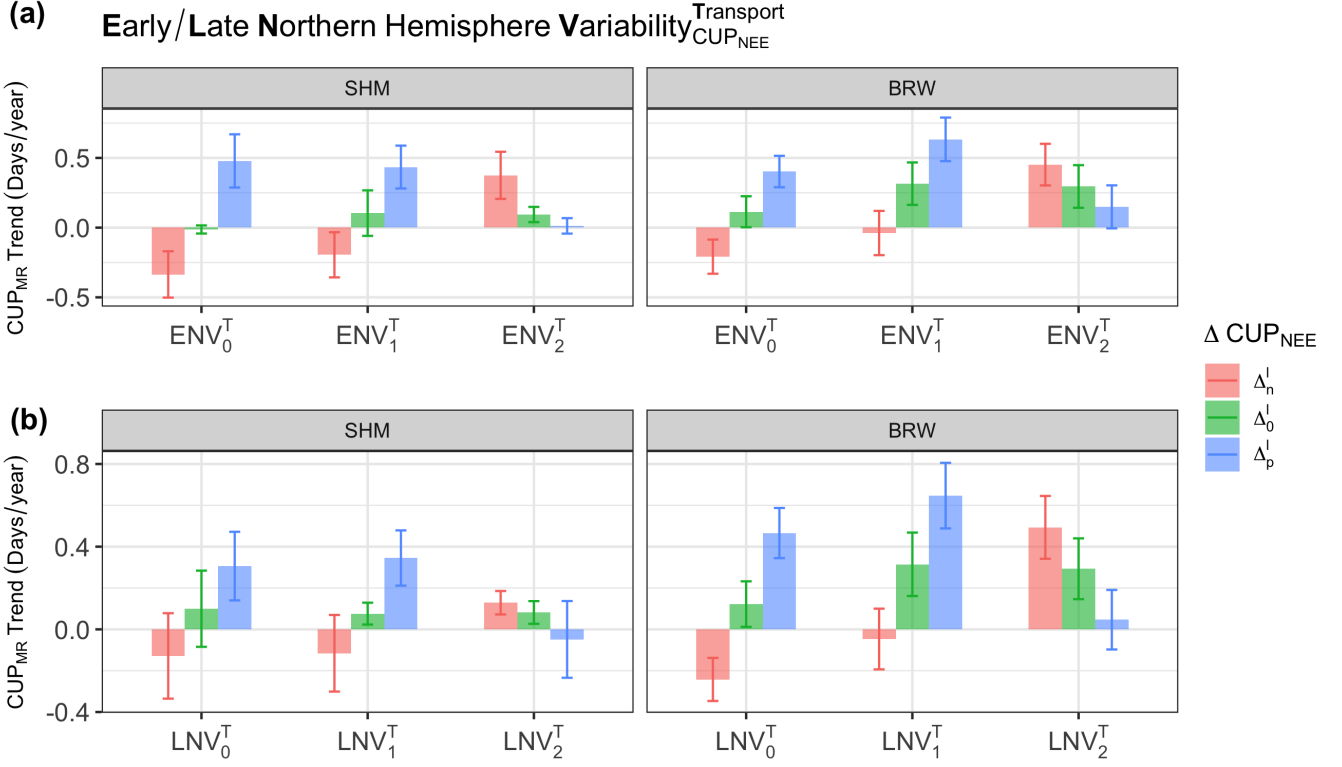
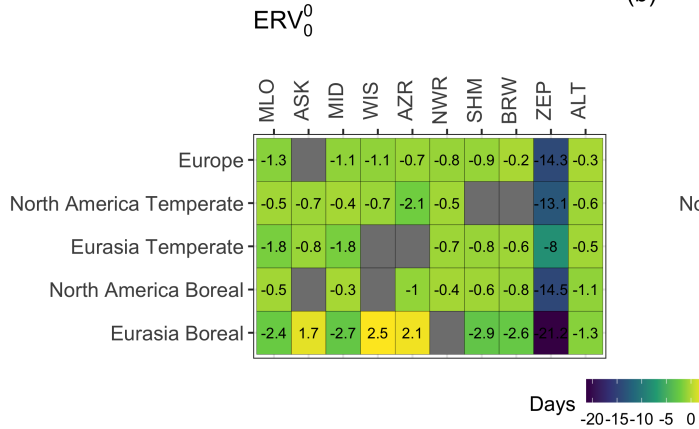


Figure 6. Sensitivity of CUP_{MR} to the applied long-term trend in CUP_{NEE} (results for sites SHM and BRW). The bars show the slope of the regression line fitted to the median CUP_{MR} from experiments ENV_x^T (a) and LNV_x^T (b), where x is 0, 1, and 2 implying no IAV in NEE flux, the actual IAV in NEE flux, and two times the actual IAV in NEE flux respectively. Error bars represent \pm one standard deviation (σ) around the estimated slope. Colours show the prescribed trend Δ_p^l (1.1 days/year) in blue, Δ_n^l (-1.1 days/year) in red and Δ_0^l (0 days/year) in green applied to CUP_{NEE} .

Furthermore, we observe that the actual IAV in the CUP_{NEE} fluxes contribute to the derived CUP_{MR} trends, however, as the IAV in the flux becomes larger, it imposes noise that makes the trends harder to detect. This is shown in experiments ENV_1^T and ENV_2^T (Fig. 6), where the actual IAV in CUP_{NEE} is retained and doubled, respectively. In experiment ENV_1^T , the CUP_{MR} trend in response to the prescribed opposite trends, Δ_p^l and Δ_n^l are distinct in sign. Even though the magnitude of the prescribed trend is the same, a large difference in magnitude can be seen between results for Δ_p^l (red bar, 0.6 days/year) and Δ_n^l (blue bar, -0.03 days/year) for example, at BRW. This can be attributed to the increasing trend from both IAV in the actual flux and transport, as indicated by the green bar for ENV_1^T . The green bars in experiment ENV_1^T (0.3 days/year) and ENV_0^T (0.1 days/year) are distinct, and their difference (0.2 days/year) is the contribution from the actual IAV in CUP_{NEE} alone. In the experiment where the IAV in CUP_{NEE} per pixel was doubled, it becomes evident that the imposed alterations in CUP_{NEE} are not

(a)



(b)

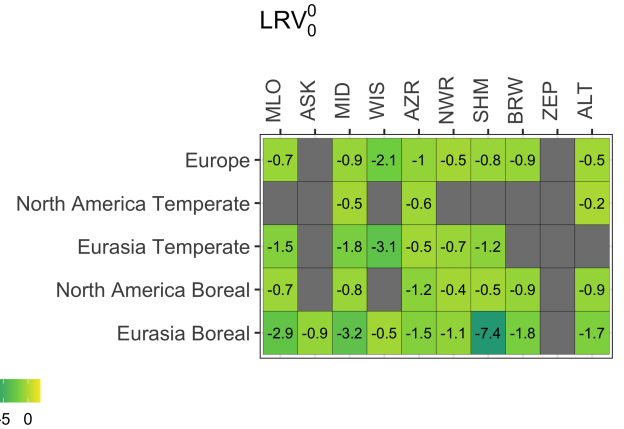


Figure 7. Regional contribution to $\Delta\text{CUP}_{\text{MR}}$. The colour and value represent the ensemble median of $\Delta\text{CUP}_{\text{MR}}$ when $\Delta\text{CUP}_{\text{NEE}}$ is -10 days, in experiment ERV_0^0 (a) and LRV_0^0 (b). Values are displayed solely for the sites where a significant difference in $\Delta\text{CUP}_{\text{MR}}$ is detected when $\Delta\text{CUP}_{\text{NEE}}$ is 0 and -10 days (p-value of Mann-Whitney test < 0.05) in the specific region (y-axis).

accurately reflected in CUP_{MR} , even at sites like BRW, which exhibited pronounced responses in other experiments (ENV_1^T and LNV_1^T).

3.4 Regional contribution to CUP_{MR}

The various Transcom3 regions of the Northern Hemisphere contribute in various degrees to the CUP_{MR} changes observed at the studied sites. The changes in the Boreal regions are partially captured at both the higher and lower latitudes like ALT, BRW, SHM, MID, and MLO. Considering both early and late phase $\Delta\text{CUP}_{\text{NEE}}$, the contribution from the Eurasian Boreal region is largely seen at SHM (-3 days in early and -7 days in the late CUP_{NEE} phase), followed by MID with (-3 in both the days early and late CUP_{NEE} phase), showing an eastward transport from the Eurasian Boreal region. Similarly, considering both the CUP_{NEE} phases, the contribution from the North American Boreal region is seen at all sites except ASK, WIS, and ZEP. In response to delayed onset, prescribed to the CUP_{NEE} in Eurasian Boreal region, a longer CUP_{MR} is calculated at ASK, WIS, and AZR (Fig. 7 (a)), suggesting that the inverse slope relation between $\Delta\text{CUP}_{\text{MR}}$ and $\Delta\text{CUP}_{\text{NEE}}$ in Sect. 3.1 might be largely from changes in the Eurasian Boreal region. In the Eurasian Temperate region, the Δ prescribed to both the early and late CUP_{NEE} phase, integrate at the lower latitude like MID, MLO, NWR, and, SHM, whereas higher latitude sites like ALT, BRW and ZEP only capture perturbations imposed during the early phase of CUP_{NEE} . The contribution from the North American Temperate region is strong during the early phase of CUP_{NEE} , while late phase changes are captured only by MID and AZR. Signals from the European region integrate well at most of the studied sites. At ZEP, a significant regional contribution from any of the studied TransCom3 regions can only be seen in the early CUP_{NEE} phase. This explains to some extent the direct

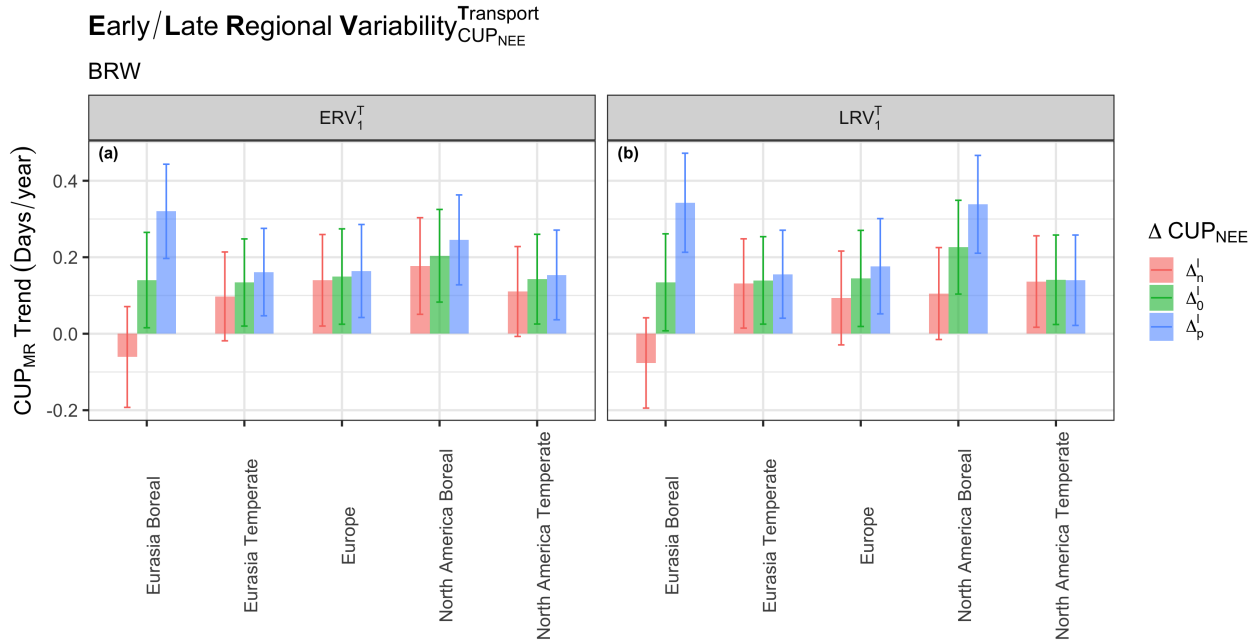


Figure 8. Regional contribution to CUP_{MR} trend detected at BRW in response to imposed long-term CUP_{NEE} trends. The bars show the slope of the regression line fitted to median CUP_{MR} from experiments ERV_1^T (a) and LRV_1^T (b). Error bars represent \pm one standard deviation (σ) around the estimated slope. [The colours represent the trend in NEE imposed in the experiment, as described in Fig. 6.](#)

relation between $\Delta\text{CUP}_{\text{MR}}$ and $\Delta\text{CUP}_{\text{NEE}}$ found only in the early phase (Sect. 3.1).

270 The long-term trend in the CUP_{MR} could not be accurately attributed to different regions even for sites like BRW that showed a predominant response to the prescribed long-term trend in CUP_{NEE} (Sect. 3.3). This can be seen from (Fig. 8). At BRW, the CUP_{MR} trends partially reflect the CUP_{NEE} trends prescribed to the Eurasian Boreal region. For example, in the early CUP_{NEE} phase, we find a change of 0.32 days/year and -0.06 days/year in response to the prescribed Δ_p^l (1.1days/year) and Δ_n^l (-1.1days/year), respectively. However, the large error bars show that the uncertainty in trend estimation is large when changes
275 are prescribed to only a given TransCom3 region.

4 Discussion

We find that changes (both fixed differences and trends) prescribed to CUP_{NEE} are reflected in CUP_{MR} simulated by TM3. However, the magnitude of the change seen in CUP_{MR} is consistently lower than the prescribed change in CUP_{NEE}, for example at BRW only about 50% of the change applied to CUP_{NEE} was reflected in $\Delta\text{CUP}_{\text{MR}}$, even in simulations with fixed
280 transport. This is contradictory to previous studies that consider the long-term CO₂ record to reflect changes in surface fluxes.

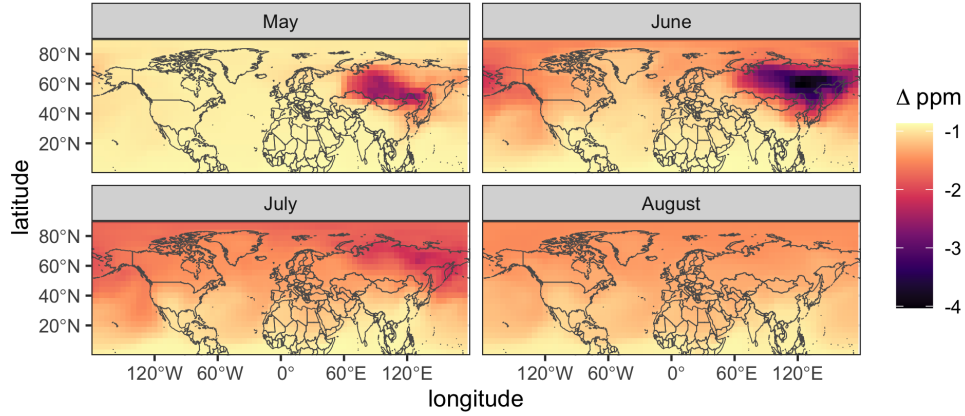


Figure 9. 2D mixing ratio fields (integrated vertically up to an altitude of 400 m and averaged per month) for when a delay of 10 days is prescribed to the CUP_{NEE} onset in the Eurasian Boreal region. The field (Δ ppm) is the difference between the 2D mixing ratio fields when ΔCUP_{NEE} of is -10 days and 0 days in the experiment ENV_0^0 , in which CUP_{NEE} from the Eurasian Boreal region was manipulated ERV_0^0 .

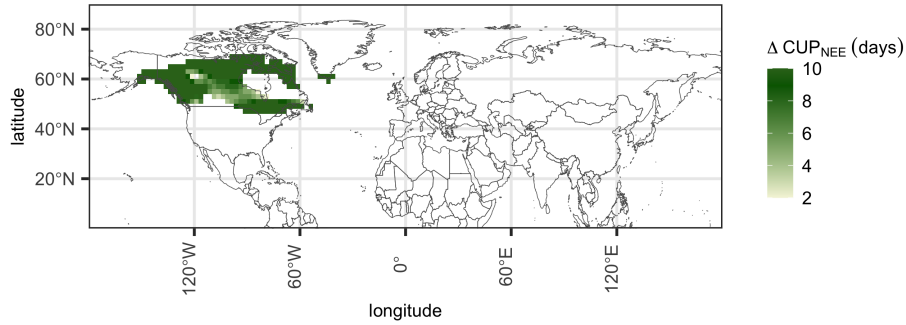


Figure 10. The ΔCUP_{NEE} variability observed across North American Boreal region over a given time period. A significant part of the region, 54% (colored pixels), has CUP_{NEE} onset between days 110 and 150. The colour intensity shows the effective ΔCUP_{NEE} during this period (days 110-150) for an applied 10-day advancement in CUP_{NEE} onset. For example, pixels with CUP_{NEE} onset on day 118 will see only a ΔCUP_{NEE} of 8 days for a prescribed 10-day advancement in CUP_{NEE} onset. The color intensity shows such difference in ΔCUP_{NEE} across the region.

For example, in Piao et al. (2008), 50% of the observed zero-crossing date variance at BRW could be accounted for by NEE variability.

We show that ~~given fixed transport~~, the reduced expression of changes in CUP_{MR} relative to CUP_{NEE} ~~arises from~~ can also
285 result from the variations in the timing of CUP_{NEE} across the different regions ~~from where the signal is integrated~~. For instance, when a delay (10 days) was applied to the CUP_{NEE} onset in the Eurasian Boreal region, the mixing ratio first reflects this change over the western part of this region in May, ~~and slowly propagates eastwards by~~. Changes in the eastern part of the domain are seen in June (Fig. 9), showing a difference in timing of the onset within the Eurasian Boreal region. Due to the difference in CUP_{NEE} timing across the pixels, the “true” ΔCUP_{NEE} of a region for a period will be different from the applied Δ , as shown
290 in Fig. 10. In a significant portion (54% pixels) of the North American Boreal region (Fig. 10), the onset of CUP_{NEE} typically occurs between days 110 and 150. If CUP_{NEE} fluxes are integrated during this period, the observed signal will represent a substantial portion of the CUP_{NEE} onset from the region. However, when a 10-day advancement in CUP_{NEE} onset is applied, the true ΔCUP_{NEE} of the region during this period is only 8.9 days (average of ΔCUP_{NEE} over the region shown in Fig. 10) and the CUP_{MR} change at the observation site would be less than the applied 10-day Δ . Below, we discuss how the sensitivity
295 of CUP_{MR} to the discrete and long-term changes in surface fluxes is affected when influenced by the interannual variability in both transport and surface fluxes.

4.1 Transport influence on CUP_{MR}

We have shown the significant role of inter-annually varying atmospheric transport in the evaluation of metrics derived from CO_2 mole fraction data. At certain sites such as ZEP and WIS, the CUP_{MR} from simulations with fixed transport failed to
300 capture the CUP_{NEE} changes, whereas in simulations with varying transport, the prescribed CUP_{NEE} changes could be partially derived from CUP_{MR} . This indicates that in a given year of meteorology used in the fixed transport simulation, the atmospheric transport is unlikely to originate from the areas where the ΔCUP_{NEE} was prescribed, while in simulations with transport variability, the meteorology in other years might have originated from these regions. Thus, the anomalies observed in CUP_{MR} in a particular year could stem from transport variability rather than anomalies in CUP_{NEE} itself, rendering mixing ratio time-series
305 less useful for studying inter-annual variations in CUP_{NEE} .

Finally, we show that due to the atmospheric transport, the source areas for a given station during the early and late CUP_{NEE} phases can be substantially different, influencing the expression of CUP_{MR} in the different CUP_{NEE} phases. For instance, our analysis (Fig. 7) shows that WIS mainly receives signals from the Northern Hemisphere land pixels only in the late CUP_{NEE}
310 phase. Consequently, at WIS, the CUP_{MR} is directly proportional solely to changes prescribed to late CUP_{NEE} phase (slope of 0.5 in $LN V_0^0$). Similarly, at ZEP, the contribution of the Northern Hemisphere landmass to ΔCUP_{MR} occurs only in the early CUP_{NEE} phase. The atmospheric transport to ZEP is dominated by the regions Eurasian Boreal and Europe, during March-May, in the following months (June-August), the air mass transport is largely ~~over the Northern Atlantic Ocean~~ confined to the Arctic

and does not extend equatorward into the continents in some years (Tunved et al., 2013; Platt et al., 2022). Our observations
315 imply that at ZEP/WIS, changes in the onset/termination of CUP_{NEE} are more effectively reflected as changes in CUP_{MR} .

4.2 Long-term trends in CUP_{MR}

The long-term trends prescribed to the CUP_{NEE} could be partially derived from CUP_{MR} at BRW and SHM, even under IAV
in atmospheric transport and CUP_{NEE} . However, when IAV in CUP_{NEE} was doubled, the prescribed trends were not captured.
This suggests that the long-term trends in the observations may be compromised when there is a higher IAV in CUP_{NEE} . The
320 contribution from atmospheric transport exhibited a CUP_{MR} trend of 0.11 days/year at BRW. This finding aligns with a study by
Murayama et al. (2007) where the IAV in transport alone caused a change of 0.16 days per year in the downward zero-crossing
date at BRW for their analysis period between 1979 and 1999.

~~Considering BRW, in experiment ENV_0^T , the difference between the green and blue bars, representing a CUP_{MR} trend of
325 0.3 days/year (Fig. 6), is solely due to the imposed trend of 1.1 day/year, showing that the surface flux changes is reduced by
a factor of 0.27. At this site, the actual IAV in CUP_{NEE} causes a CUP_{MR} trend of 0.2 days/ year (see Sect. 3.3). Considering
the reducing factor, a change of approximately 0.7 days/year might be occurring in the surface fluxes.~~ With warming, a longer
growing season is observed in the high latitudes (e.g. Park et al. (2016), 2.6 days per decade). A longer growing season does
not necessarily mean an increase in CUP_{NEE} or CUP_{MR} as they are determined by both photosynthesis and respiration. The
330 existing literature on the CUP_{NEE} changes in the Northern Hemisphere based on CUP_{MR} varies from increasing (Murayama
et al., 2007) to neutral (Barichivich et al., 2012) to decreasing (Piao et al., 2008; Fu et al., 2017). The complications in inter-
preting CUP_{NEE} changes arise mostly when directly assessing the CUP from CO_2 mixing ratio. Therefore, CO_2 observations
should preferably be interpreted following a formal inverse estimate of the corresponding surface NEE. It is then possible to
account for the inter-annual variability, trends, and delays imposed by the slow atmospheric mixing. Nevertheless, the ability
335 of such inversions to constrain regional changes in NEE can only be improved with an expanded observation network.

4.3 Regional contribution to CUP_{MR}

The regions contributing to the integrated signal, at various observation sites are influenced by atmospheric transport to these
locations. From the idealized simulations with no IAV in transport nor CUP_{NEE} it turned out that at sites like ALT, BRW, SHM,
and MLO, a significant contribution from Boreal and Temperate regions could be calculated, indicating that these remote sites
340 receive well-mixed signals from higher and mid-latitude regions in the Northern Hemisphere with strong seasonality. We calcu-
late that the contribution from mid-latitude is significant at the sites in the Boreal region (e.g. ALT and BRW in early CUP_{NEE}
phase) in line with Barnes et al. (2016). They found that the seasonal cycle observed at higher latitude sites is most sensitive
to changes in the seasonality of mid-latitude surface emissions, however, we do not find that the mid-latitude influence is more
than the Boreal region influences at higher latitude sites. At ZEP, strong signals from both Eurasian and North American regions
345 dominate during the early CUP_{NEE} phase (Fig. 7), and an amplification of the CUP_{MR} signal is found. Further, a significant
change in the regional contribution is found between the early and late CUP_{NEE} phases, shifting from continental in the early

CUP_{NEE} phase to ocean signals in parts of the late CUP_{NEE} phase (Sect. 4.1). This change explains the significant difference in $\Delta\text{CUP}_{\text{MR}}$ to $\Delta\text{CUP}_{\text{NEE}}$ during different phases, as shown in Fig. 4. At WIS, ASK, and AZR, when a delayed onset is imposed on the CUP_{NEE} from Eurasian Boreal regions, a positive $\Delta\text{CUP}_{\text{MR}}$ (i.e., an extension in CUP_{MR}) is calculated. These sites are
350 located in the temperate regions. The CO₂ 2D mixing ratio fields (Fig. 9) reveal that changes imposed on the Boreal region propagate partially to the lower latitudes (around 30 degrees north) later in the CUP_{NEE} phase. Thereby the delay imposed on the CUP_{NEE} of the Eurasian Boreal region in May integrates at the lower latitude region (near to the location of WIS, ASK, and AZR) only later in July, delaying and extending the CUP_{MR}.

355 When the long-term trends were applied to specific regions, the slope estimated from CUP_{MR} had large uncertainty due to the influence of IAV in transport and CUP_{NEE}. Furthermore, the flux manipulation strictly within the boundaries of the TransCom3 region in our experiments may have substantially limited the regions from which the signals reach the sites. In the real world, regional boundaries are more diffuse, and the footprint of the site provides a more accurate estimate of the regions contributing to the observed signals. Nonetheless, this aspect falls outside the scope of the present study.

360 The changes in the CO₂ mixing ratio time series from the Northern Hemisphere give a larger spatial perspective of the CUP_{NEE} changes. However, results from idealized simulations suggest that they are influenced by atmospheric transport IAV, seasonal changes in atmospheric transport, and IAV in the biospheric fluxes. We find a significant damping of the changes that were imposed on the CUP_{NEE}, from the integration of signals from different regions that have varied timing and suggest a more
365 intense change in the local spatial scales. With the constraints in NEE flux manipulation, imposed by the presence of local maxima and insufficient data points for Δ changes in the early and late CUP_{NEE} (Sect. 2.1), the simulations in this study do not accurately represent the real-world scenarios. In the real world, the changes in CUP_{NEE} are asynchronous across space. Although we broadly examined the influence of different TransCom3 regions, conducting more dedicated footprint analyses of the studied sites may offer further insights into the signals studied here.

370 5 Conclusions

Our analysis reveals that at well-studied sites such as MLO, BRW, and ALT, only circa 50% of the prescribed changes in the CUP_{NEE} fluxes were reflected in CUP_{MR}. In simulations with inter-annually varying meteorology, the signals were better captured at a few sites like ZEP and WIS, showing the significant influence of IAV in atmospheric transport. At BRW, 20% of the observed trend could be attributed to the IAV in transport. Furthermore, our findings suggest that the changes estimated
375 in CUP_{MR}, subsequent to the separation of atmospheric transport influence, are likely to underestimate the actual magnitude of signals from the surface changes. This is because of the damping due to the integration of asynchronous CUP_{NEE} timing across different regions. While sites like BRW and SHM captured the prescribed long-term changes, they proved insensitive when IAV in CUP_{NEE} was doubled. Furthermore, trends prescribed to individual TransCom3 regions were not captured by the evaluated sites, showing the long-term changes in the seasonal cycle of time series.

380 *Code and data availability.* The NEE flux used here (Rödenbeck et al., 2003) is available from the Jena CarboScope website at https://www.bgc-jena.mpg.de/CarboScope/?ID=sEXT_ocNEET. The code used for manipulation of the flux is available from the corresponding author on request.

Appendix

Table A1. Sensitivity of CUP_{MR} to the applied long-term trend in CUP_{NEE} for the different sites (excluding SHM and BRW). The first column shows the sites, the second column describes the prescribed trend Δ_x^l applied to CUP_{NEE} , and the other columns describe the different experiments, as detailed in the caption of Fig. 6. The values show the slope of the regression line fitted to the median $CUP_{MR} \pm$ one standard deviation (σ) around the estimated slope (in units of days/year) for the experiments indicated by the column names.

Site	Δ_x^l	ENV_0^T	ENV_1^T	ENV_2^T	LVN_0^T	LVN_1^T	LVN_2^T
MLO	Δ_p^l	0.07 ± 0.04	0.10 ± 0.05	0.00 ± 0.03	0.03 ± 0.04	0.06 ± 0.05	-0.05 ± 0.05
MLO	Δ_0^l	0.00 ± 0.03	0.02 ± 0.03	0.02 ± 0.03	0.00 ± 0.03	0.02 ± 0.03	0.00 ± 0.05
MLO	Δ_p^l	-0.14 ± 0.03	-0.08 ± 0.05	0.07 ± 0.05	-0.11 ± 0.04	-0.05 ± 0.05	0.05 ± 0.05
ASK	Δ_p^l	0.07 ± 0.07	0.31 ± 0.11	0.01 ± 0.07	0.13 ± 0.08	0.10 ± 0.08	0.06 ± 0.11
ASK	Δ_0^l	0.02 ± 0.05	0.05 ± 0.08	0.06 ± 0.08	0.02 ± 0.05	0.05 ± 0.08	0.05 ± 0.09
ASK	Δ_p^l	-0.08 ± 0.06	0.00 ± 0.07	0.26 ± 0.11	-0.11 ± 0.09	0.33 ± 0.28	0.09 ± 0.09
MID	Δ_p^l	0.05 ± 0.04	0.09 ± 0.04	0.03 ± 0.03	0.05 ± 0.05	0.06 ± 0.04	0.03 ± 0.03
MID	Δ_0^l	0.04 ± 0.04	0.03 ± 0.03	0.03 ± 0.03	0.03 ± 0.04	0.03 ± 0.03	0.03 ± 0.03
MID	Δ_p^l	0.02 ± 0.04	0.02 ± 0.03	0.04 ± 0.03	0.03 ± 0.04	0.05 ± 0.04	0.03 ± 0.03
WIS	Δ_p^l	0.08 ± 0.13	0.17 ± 0.13	-0.12 ± 0.11	-0.35 ± 0.15	-0.06 ± 0.13	0.00 ± 0.12
WIS	Δ_0^l	-0.25 ± 0.14	-0.02 ± 0.12	-0.01 ± 0.12	-0.23 ± 0.13	-0.02 ± 0.12	-0.02 ± 0.13
WIS	Δ_p^l	-1.02 ± 0.2	-0.19 ± 0.12	0.09 ± 0.12	-0.12 ± 0.13	0.03 ± 0.16	-0.03 ± 0.13
AZR	Δ_p^l	0.01 ± 0.03	0.01 ± 0.05	-0.01 ± 0.03	0.00 ± 0.02	0.00 ± 0.05	-0.01 ± 0.05
AZR	Δ_0^l	0.01 ± 0.03	-0.01 ± 0.03	-0.01 ± 0.03	0.00 ± 0.02	0.00 ± 0.03	0.00 ± 0.03
AZR	Δ_p^l	0.01 ± 0.02	0.00 ± 0.03	0.00 ± 0.03	-0.02 ± 0.04	0.00 ± 0.07	-0.01 ± 0.03
NWR	Δ_p^l	0.03 ± 0.06	0.44 ± 0.29	0.03 ± 0.13	0.02 ± 0.06	0.05 ± 0.23	0.24 ± 0.22
NWR	Δ_0^l	0.01 ± 0.06	0.05 ± 0.17	0.04 ± 0.14	0.01 ± 0.06	0.16 ± 0.21	0.04 ± 0.16
NWR	Δ_p^l	0.01 ± 0.06	0.03 ± 0.14	0.06 ± 0.16	0.01 ± 0.06	0.26 ± 0.23	0.07 ± 0.24
ZEP	Δ_p^l	0.18 ± 0.04	0.35 ± 0.06	0.05 ± 0.04	0.11 ± 0.04	0.22 ± 0.06	0.15 ± 0.06
ZEP	Δ_0^l	0.02 ± 0.03	0.09 ± 0.04	0.08 ± 0.04	0.02 ± 0.03	0.08 ± 0.04	0.08 ± 0.04
ZEP	Δ_p^l	-0.04 ± 0.03	0.02 ± 0.05	0.12 ± 0.04	0.00 ± 0.04	0.51 ± 0.15	0.09 ± 0.04
ALT	Δ_p^l	0.05 ± 0.03	0.19 ± 0.06	0.00 ± 0.03	0.10 ± 0.05	0.18 ± 0.06	0.02 ± 0.06
ALT	Δ_0^l	0.00 ± 0.03	0.05 ± 0.04	0.05 ± 0.04	-0.01 ± 0.03	0.05 ± 0.04	0.05 ± 0.04
ALT	Δ_p^l	-0.05 ± 0.03	-0.02 ± 0.06	0.07 ± 0.04	-0.07 ± 0.04	-0.01 ± 0.06	0.13 ± 0.06

Author contributions. The coding and analysis were performed by TK with the contributions of JM. The study was conceptualized by JM,
385 AB, and WP with contributions from MR. The original manuscript was drafted by TK, which was reviewed and edited by AB, WP, JM, and
MR.

Competing interests. The contact author has declared that none of the authors has any competing interests.

Acknowledgements. We thank Christian Rödenbeck for providing access to the NEE flux data from the Jena CarboScope Inversion, as well
as for his assistance in resolving queries related to running the TM3 transport model. We acknowledge the assistance of ChatGPT 3.5 for its
390 support in refining the grammatical structure and phrasing of this publication.

References

- Barichivich, J., Briffa, K., Osborn, T., Melvin, T., and Caesar, J.: Thermal growing season and timing of biospheric carbon uptake across the Northern Hemisphere, *Global Biogeochemical Cycles*, 26, 4015–, <https://doi.org/10.1029/2012GB004312>, 2012.
- Barichivich, J., Briffa, K. R., Myneni, R. B., Osborn, T. J., Melvin, T. M., Ciais, P., Piao, S., and Tucker, C.: Large-scale variations in the vegetation growing season and annual cycle of atmospheric CO₂ at high northern latitudes from 1950 to 2011, *Global Change Biology*, 19, 3167–3183, <https://doi.org/10.1111/gcb.12283>, 2013.
- Barlow, J. M., Palmer, P. I., Bruhwiler, L. M., and Tans, P.: Analysis of CO₂ mole fraction data: first evidence of large-scale changes in CO₂ uptake at high northern latitudes, *Atmospheric Chemistry and Physics*, 15, 13 739–13 758, <https://doi.org/10.5194/acp-15-13739-2015>, 2015.
- Barnes, E. A., Parazoo, N., Orbe, C., and Denning, A. S.: Isentropic transport and the seasonal cycle amplitude of CO₂, *Journal of Geophysical Research: Atmospheres*, 121, 8106–8124, <https://doi.org/10.1002/2016JD025109>, 2016.
- Buermann, W., Forkel, M., O’Sullivan, M., Sitch, S., Friedlingstein, P., Haverd, V., Jain, A. K., Kato, E., Kautz, M., Lienert, S., Lombardozzi, D., Nabel, J. E. M. S., Tian, H., Wiltshire, A. J., Zhu, D., Smith, W. K., and Richardson, A. D.: Widespread seasonal compensation effects of spring warming on northern plant productivity, *Nature*, 562, 110–114, <https://doi.org/10.1038/s41586-018-0555-7>, 2018.
- Churkina, G., Schimel, D., Braswell, B. H., and Xiao, X.: Spatial analysis of growing season length control over net ecosystem exchange, *Global Change Biology*, 11, 1777–1787, <https://doi.org/10.1111/j.1365-2486.2005.001012.x>, 2005.
- Ciais, P., Tan, J., Wang, X., Roedenbeck, C., Chevallier, F., Piao, S.-L., Moriarty, R., Broquet, G., Le Quéré, C., Canadell, J. G., Peng, S., Poulter, B., Liu, Z., and Tans, P.: Five decades of northern land carbon uptake revealed by the interhemispheric CO₂ gradient, *Nature*, 568, 221–225, <https://doi.org/10.1038/s41586-019-1078-6>, 2019.
- Forkel, M., Carvalhais, N., Rödenbeck, C., Keeling, R., Heimann, M., Thonicke, K., Zaehle, S., and Reichstein, M.: Enhanced seasonal CO₂ exchange caused by amplified plant productivity in northern ecosystems, *Science*, 351, 696–699, <https://doi.org/10.1126/science.aac4971>, 2016.
- Fu, Z., Stoy, P. C., Luo, Y., Chen, J., Sun, J., Montagnani, L., Wohlfahrt, G., Rahman, A. F., Rambal, S., Bernhofer, C., Wang, J., Shirkey, G., and Niu, S.: Climate controls over the net carbon uptake period and amplitude of net ecosystem production in temperate and boreal ecosystems, *Agricultural and Forest Meteorology*, 243, 9–18, <https://doi.org/10.1016/j.agrformet.2017.05.009>, 2017.
- Fu, Z., Stoy, P. C., Poulter, B., Gerken, T., Zhang, Z., Waktulcho, G., and Niu, S.: Maximum carbon uptake rate dominates the interannual variability of global net ecosystem exchange, *Global Change Biology*, 25, 3381–3394, <https://doi.org/10.1111/gcb.14731>, 2019.
- Gill, A. L., Gallinat, A. S., Sanders-DeMott, R., Rigden, A. J., Short Gianotti, D. J., Mantooth, J. A., and Templer, P. H.: Changes in autumn senescence in northern hemisphere deciduous trees: a meta-analysis of autumn phenology studies, *Annals of Botany*, 116, 875–888, <https://doi.org/10.1093/aob/mcv055>, 2015.
- Gonsamo, A., Chen, J. M., Wu, C., and Dragoni, D.: Predicting deciduous forest carbon uptake phenology by upscaling FLUXNET measurements using remote sensing data, *Agricultural and Forest Meteorology*, 165, 127–135, <https://doi.org/10.1016/j.agrformet.2012.06.006>, 2012.
- Graven, H. D., Keeling, R. F., Piper, S. C., Patra, P. K., Stephens, B. B., Wofsy, S. C., Welp, L. R., Sweeney, C., Tans, P. P., Kelley, J. J., Daube, B. C., Kort, E. A., Santoni, G. W., and Bent, J. D.: Enhanced seasonal exchange of CO₂ by northern ecosystems since 1960, *Science*, 341, 1085–9, <https://doi.org/10.1126/science.1239207>, 2013.

- Gurney, K. R., Law, Rachel M. and Denning, A. S. R. P. J. B. D., Bousquet, P., Bruhwiler, L., Chen, Y.-H., Ciais, P., Fan, S., Fung, I. Y., Gloor, M., Heimann, M., Higuchi, K., John, J., Maki, T., Maksyutov, S., Masarie, K., Peylin, P., Prather, M., Pak, B. C., Randerson, J., Sarmiento, J., Taguchi, S., Takahashi, T., and Yuen, C.-W.: Towards robust regional estimates of CO₂ sources and sinks using atmospheric transport models, *Nature*, 415, 626–630, <https://doi.org/10.1038/415626a>, 2002.
- 430 Heimann, H. and Körner, S.: The global atmospheric tracer model TM3., Technical Reports - Max-Planck-Institut für Biogeochemie 5, 5, 131, 2003.
- Jin, Y., Keeling, R. F., Rödenbeck, C., Patra, P. K., Piper, S. C., and Schwartzman, A.: Impact of Changing Winds on the Mauna Loa CO₂ Seasonal Cycle in Relation to the Pacific Decadal Oscillation, *Journal of Geophysical Research: Atmospheres*, 127, e2021JD035 892, <https://doi.org/https://doi.org/10.1029/2021JD035892>, e2021JD035892 2021JD035892, 2022.
- 435 Jung, M., Schwalm, C., Migliavacca, M., Walther, S., Camps-Valls, G., Koirala, S., Anthoni, P., Besnard, S., Bodesheim, P., Carvalhais, N., Chevallier, F., Gans, F., Goll, D. S., Haverd, V., Köhler, P., Ichii, K., Jain, A. K., Liu, J., Lombardozzi, D., Nabel, J. E. M. S., Nelson, J. A., O’Sullivan, M., Pallandt, M., Papale, D., Peters, W., Pongratz, J., Rödenbeck, C., Sitch, S., Tramontana, G., Walker, A., Weber, U., and Reichstein, M.: Scaling carbon fluxes from eddy covariance sites to globe: synthesis and evaluation of the FLUXCOM approach, *Biogeosciences*, 17, 1343–1365, <https://doi.org/10.5194/bg-17-1343-2020>, 2020.
- 440 Kariyathan, T., Bastos, A., Marshall, J., Peters, W., Tans, P., and Reichstein, M.: Reducing errors on estimates of the carbon uptake period based on time series of atmospheric CO₂, *Atmospheric Measurement Techniques*, 16, 3299–3312, <https://doi.org/10.5194/amt-16-3299-2023>, 2023.
- Keeling, C. D., Chin, J. F. S., and Whorf, T. P.: Increased activity of northern vegetation inferred from atmospheric CO₂ measurements, *Nature*, 382, 146–149, 1996.
- 445 Lintner, B. R., Buermann, W., Koven, C. D., and Fung, I. Y.: Seasonal circulation and Mauna Loa CO₂ variability, *Journal of Geophysical Research: Atmospheres*, 111, <https://doi.org/10.1029/2005JD006535>, 2006.
- Murayama, S., Higuchi, K., and Taguchi, S.: Influence of atmospheric transport on the inter-annual variation of the CO₂ seasonal cycle downward zero-crossing, *Geophysical Research Letters*, 34, <https://doi.org/10.1029/2006GL028389>, 2007.
- 450 Park, T., Ganguly, S., Tømmervik, H., Euskirchen, E. S., Høgda, K.-A., Karlsen, S. R., Brovkin, V., Nemani, R. R., and Myneni, R. B.: Changes in growing season duration and productivity of northern vegetation inferred from long-term remote sensing data, *Environmental Research Letters*, 11, 084 001, <https://doi.org/10.1088/1748-9326/11/8/084001>, 2016.
- Piao, S., Ciais, P., Friedlingstein, P., Peylin, P., Reichstein, M., Luyssaert, S., Margolis, H., Fang, J., Barr, A., Chen, A., Grelle, A., Hollinger, D., Laurila, T., Lindroth, A., Richardson, A., and Vesala, T.: Net carbon dioxide losses of northern ecosystems in response to autumn warming, *Nature*, 451, 49–52, <https://doi.org/10.1038/nature06444>, 2008.
- 455 Piao, S., Liu, Z., Wang, T., Peng, S., Ciais, P., Huang, M., Ahlstrom, A., Burkhardt, J. F., Chevallier, F., Janssens, I. A., Jeong, S.-J., Lin, X., Mao, J., Miller, J., Mohammat, A., Myneni, R. B., Peñuelas, J., Shi, X., Stohl, A., Yao, Y., Zhu, Z., and Tans, P. P.: Weakening temperature control on the interannual variations of spring carbon uptake across northern lands, *Nature Climate Change*, 7, 359–363, <https://doi.org/10.1038/nclimate3277>, 2017.
- 460 Piao, S., Liu, Q., Chen, A., Janssens, I. A., Fu, Y., Dai, J., Liu, L., Lian, X., Shen, M., and Zhu, X.: Plant phenology and global climate change: Current progresses and challenges, *Global Change Biology*, 25, 1922–1940, <https://doi.org/10.1111/gcb.14619>, 2019.
- Platt, S. M., Hov, Ø., Berg, T., Breivik, K., Eckhardt, S., Eleftheriadis, K., Evangeliou, N., Fiebig, M., Fisher, R., Hansen, G., Hansson, H.-C., Heintzenberg, J., Hermansen, O., Heslin-Rees, D., Holmén, K., Hudson, S., Kallenborn, R., Krejci, R., Krognen, T., Larssen, S., Lowry, D., Lund Myhre, C., Lunder, C., Nisbet, E., Nizzetto, P. B., Park, K.-T., Pedersen, C. A., Aspmo Pfaffhuber, K., Röckmann, T.,

- 465 Schmidbauer, N., Solberg, S., Stohl, A., Ström, J., Svendby, T., Tunved, P., Tørnkvist, K., van der Veen, C., Vratolis, S., Yoon, Y. J., Yttri, K. E., Zieger, P., Aas, W., and Tørseth, K.: Atmospheric composition in the European Arctic and 30 years of the Zeppelin Observatory, Ny-Ålesund, *Atmospheric Chemistry and Physics*, 22, 3321–3369, <https://doi.org/10.5194/acp-22-3321-2022>, 2022.
- Rödenbeck, C., Houweling, S., Gloor, M., and Heimann, M.: CO₂ flux history 1982–2001 inferred from atmospheric data using a global inversion of atmospheric transport, *Atmospheric Chemistry and Physics*, 3, 1919–1964, <https://doi.org/10.5194/acp-3-1919-2003>, 2003.
- 470 Shen, M., Wang, S., Jiang, N., Sun, J., Cao, R., Ling, X., Fang, B., Zhang, L., Zhang, L., Xu, X., Lv, W., Li, B., Sun, Q., Meng, F., Jiang, Y., Dorji, T., Fu, Y., Iler, A., Vitasse, Y., Steltzer, H., Ji, Z., Zhao, W., Piao, S., and Fu, B.: Plant phenology changes and drivers on the Qinghai–Tibetan Plateau, *Nature Reviews Earth & Environment*, 3, 633–651, <https://doi.org/10.1038/s43017-022-00317-5>, 2022.
- Tunved, P., Ström, J., and Krejci, R.: Arctic aerosol life cycle: linking aerosol size distributions observed between 2000 and 2010 with air mass transport and precipitation at Zeppelin station, Ny-Ålesund, Svalbard, *Atmospheric Chemistry and Physics*, 13, 3643–3660, <https://doi.org/10.5194/acp-13-3643-2013>, 2013.
- 475 van der Woude, A. M., Peters, W., Joetzjer, E., Lafont, S., Koren, G., Ciaia, P., Ramonet, M., Xu, Y., Bastos, A., Botía, S., Sitch, S., de Kok, R., Kneuer, T., Kubistin, D., Jacotot, A., Loubet, B., Herig-Coimbra, P.-H., Loustau, D., and Luijkx, I. T.: Temperature extremes of 2022 reduced carbon uptake by forests in Europe, *Nature Communications*, 14, 6218, <https://doi.org/10.1038/s41467-023-41851-0>, 2023.
- Walther, S., Besnard, S., Nelson, J. A., El-Madany, T. S., Migliavacca, M., Weber, U., Carvalhais, N., Ermida, S. L., Brümmer, C., Schrader, F., Prokushkin, A. S., Panov, A. V., and Jung, M.: Technical note: A view from space on global flux towers by MODIS and Landsat: the FluxnetEO data set, *Biogeosciences*, 19, 2805–2840, <https://doi.org/10.5194/bg-19-2805-2022>, 2022.
- 480 Wang, X., Sun, Z., Lu, S., and Zhang, Z.: Comparison of Phenology Estimated From Monthly Vegetation Indices and Solar-Induced Chlorophyll Fluorescence in China, *Frontiers in Earth Science*, 10, <https://doi.org/10.3389/feart.2022.802763>, 2022.
- Zeng, L., Wardlow, B. D., Xiang, D., Hu, S., and Li, D.: A review of vegetation phenological metrics extraction using time-series, multispectral satellite data, *Remote Sensing of Environment*, 237, 111 511, <https://doi.org/10.1016/j.rse.2019.111511>, 2020.
- 485 Zhou, X., Geng, X., Yin, G., Hänninen, H., Hao, F., Zhang, X., and H. Fu, Y.: Legacy effect of spring phenology on vegetation growth in temperate China, *Agricultural and Forest Meteorology*, 281, 107 845, <https://doi.org/10.1016/j.agrformet.2019.107845>, 2020.
- Zhu, W., Tian, H., Xu, X., Pan, Y., Chen, G., and Lin, W.: Extension of the growing season due to delayed autumn over mid and high latitudes in North America during 1982–2006, *Global Ecology and Biogeography*, 21, 260–271, <https://doi.org/10.1111/j.1466-8238.2011.00675.x>, 2012.
- 490